A parametric study of adhesive bonded joints with composite material using black-box and grey-box machine learning methods: deep neuron networks and genetic programming

Zewen Gu[a], Yiding Liu[b], Darren J. Hughes[b], Jianqiao Ye[a], Xiaonan Hou[a,*]

[a] Department of Engineering, Engineering Building, Lancaster University, Lancaster, LA1 4YW, UK

[b] WMG, University of Warwick, Coventry, CV4 7AL, UK

[*] Corresponding author. Email address: x.hou2@lancaster.ac.uk; Tel: +44 (0)1524 593314

Abstract

The aerospace, automotive and marine industries have witnessed a rapid increase of using adhesive bonded joints due to their advantages in joining dissimilar and/or new engineering materials. Joint strength is the key property in evaluating the capability of the adhesive joint. In this paper, developments of black-box and grey-box machine learning (ML) models are presented to allow accurate predictions of the failure load of single lap joints by considering a mix of continuous and discrete design (geometry and material) variables. Firstly, the failure loads of 300 single lap joint samples with different geometry/material parameters are calculated by FE models to generate a data set of which accuracy is validated by experimental results. Then, a deep neuron network (black-box) and a genetic programming (grey-box) model are developed for accurately predicting the failure load of the joint. Based on both ML models, a case study is conducted to explore the relationships between specific design variables and overall mechanical performances of the single lap adhesive joint, and optimal designs of structure and material can be obtained.

Keywords: adhesive bonded joint; composite material; finite element model; genetic programming; deep neuron network

1. Introduction

The long-term financial and environmental viability has pushed aviation and transportation industries to engage in the application of a lightweight multi-material design strategy for primary structures [1]. This has stimulated the application of structural adhesives due to their compatibility with a wide range of material types and the possibility of combining multi-material structures. Adhesive joining also exhibits high strength-to-weight ratio, uniform stress transfer, design flexibility, damage tolerance, and crash/fatigue resistance over conventional joining methods [2].

The performance of adhesive bonded joints depends on several effective design variables such as surface treatment, material parameters (properties of adhesive and adherend), and geometrical configuration (adhesive thickness, overlap length, stacking sequence, fillet etc.), which have been studied intensively by using conventional analysis methods, such as analytical model, numerical model and experiment. For instance, da Silva et al. [3] investigated the importance of geometric parameters on the lap shear strength respectively. Similar works have also been done by many other researchers [4-7], either by adjusting the geometric dimensions or the combination of materials within the joints. Their works contribute to the science of adhesive bonded joints to understand the effects of individual key design factors.

However, most of the existing studies use “one-factor-at-a-time” (OFAT) technique, which only investigates the effects of one design variable on responses of the interests rather than assessing the mutual effect of all effective variables on the overall performances. Actually, the mutual effect of design variables of an adhesive bonded joint is very complicated and erratic. Therefore, the latest studies start to use evidence-based machine learning techniques to replace the conventional numerical and experimental methods to investigate the mutual effects of design variables of the adhesive joint. Artificial neuron network (ANN) is one of these promising

machine learning techniques. ANN tends to find the relationships between parameters and outputs based on a specific form of activation function. The first interest on artificial neurons was emerged after McCulloch and Pitts published their work in 1943 [8]. Inspired by networks of biological neurons, artificial neurons were modelled by these biological neurons. At present, there are a few studies using the technique in analysis of structural joints. Mashrei [9] predicted the bond strength of fibre reinforced polymers to concrete joints using a back-propagation neuron networks. The method was then applied to predict the strength of a single lap joint by considering the effects of width and length of adherends [10], to predict the adhesive bonded pultruded composites by considering different bonding angles [11] and to predict the strength of adhesive bonded single lap composite joints with varying overlap length and adhesive thickness [12]. The results of these studies show that the efficiency of ANN method is very high in comparison with the results of analytical and multiple linear regression models. However, only continuous and basic geometry parameters were considered in these studies.

Another machine learning technique, which was used in analysis of adhesive joints, is Genetic Programming (GP). The technique is a variant of genetic algorithm, which attracted many attentions of researchers after its first application by Forsyth [13] in pattern recognition. Initially, researchers used genetic programming in formulating capacities of different types of steel beams [14-16], the distortional buckling stress of steels [17] and mechanical properties of rock [18]. Then, genetic programming also demonstrated its potential in tackling complex nonlinear structural engineering problems [19, 20] and effects of microstructure on overall mechanical performance of composite materials [21]. Recently, genetic programming technique started to be used to develop meta-models for design optimization of composite lattice materials [22] and functional structures [23, 24]. However, there are not many studies using GP in analysis of the performance of lap joints. According to the author's knowledge, the only work has been done by Al-Mosawe et al. [25] and Liu et al. [26]. In Ref [25], GP was used to predict

the bond strength of a double strap joint under various loading rates, which is made of carbon fibre reinforced polymers and steel adherends. However, the work only considered limited linear continuous variables in the analysis, such as bond length, loading rate and Young's modulus of adherends. In Ref [26], GP was used to analyse the mode I vs. mode II strain energy release rate ratio at the crack tip in a single lap joint and an equation was proposed related with the material properties and thickness of the adherends and adhesive.

Although some efforts have been made to use machine learning techniques in analysis of adhesive lap joints, the existing studies are generally based on very simple cases, which only consider limited continuous variables. So far, there is no well received systematic study in this field that involves all possible design variables of a joint in a machine learning model, especially the discrete variables such as the type of adherends and adhesive. Hence, this study aims to develop two machine learning models for predicting the performance of single lap joints based on both deeper ANN (DNN) and genetic programming techniques, which could consider the effects of mixed continuous and discrete design variables of the joints. The training and testing data of the machine learning models are sampled by Latin Hypercube method and generated by Finite Element (FE) models. Based on the results, the performances of the two machine learning models are analysed, and their potential applications are also discussed.

2. Parametric FE model and validation

To generate the data set for training and testing machine learning models, a parametric FE model is developed based on surface-based Cohesive Zone Method (CZM) in Ansys Workbench to calculate the failure load of a single lap joint under a static tensile loading. In the model, the geometry parameters and material parameters of the constituents (adherends and adhesive) of the joint are defined as variables. The schematic of the parametric geometry model is shown in Figure 1, which illustrates the variable geometric parameters: the thickness of top

and bottom adherends (T_1, T_2), the bond overlap length (L_a) and the thickness of adhesive (T_a), and the variable material parameters: the materials of the top adherend (M_t), the bottom adherend (M_b) and the adhesive (M_a). The adherend length and the tab length are fixed at 100 and 25 mm with a joint width of 25 mm, according to the ASTM D5868 standard.

The mesh of the model is shown in Figure 2. Four-node plane-strain elements are used for both the adherends and adhesive. The mesh sizes used in the adhesive and the other areas are 0.1 mm and 0.4 mm, respectively, after a mesh convergence study to save computational time. The adhesive section is modelled as two separate parts, with the neutral axis defined by contact debonding with surface-based cohesive properties. The material properties of adherends and the cohesive properties of the adhesive used for the parametric analysis are summarised in Section 3 and illustrated in Table 1. The displacements and rotations of the entire nodes at one (left) end are restrained in all direction and the other (right) end are fixed in *y*-direction and *z*-direction movements and rotations, as indicated in Figure 2. A displacement is applied to the (right) end nodes till final failure. The models are computed considering non-linear geometric analysis.

To validate the accuracy of the developed FE model, two categories of single lap joints (identical aluminium and composite joints) were fabricated and tested. The aluminium used in the joint is 6082 T6, which is a commonly series for automotive industry and the adhesive used for bonding the aluminium joints is Araldite® 2015, which is a two-component, room temperature curing structural adhesive providing a resilient bond. For the composite joints, the adherend was made of unidirectional Hexcel® 8552/IM7 pre-preg with a quasi-isotropic stacking sequence of $[0/45/90/-45]_S$. The properties of the composite were determined in previous studies [27, 28] and the adhesive used in the joints is Cytec FM® 94 modified epoxy adhesive film (a moisture resistant adhesive designed for use in high temperature environments). The material properties of the adherends and the adhesives are summarized in Table 1. Both joint categories have adherend and adhesive thicknesses of 2 and 0.25 mm, and an

overlap length of 25 mm. In addition, a slightly different joint geometries were applied to validate the strategy of the developed FE model to fit various joints designs. For the composite and the aluminium joints, the adherend lengths are 114 mm and 100 mm respectively, and the widths of the composite and aluminium joints are 50 mm and 25 mm respectively.

During the manufacturing of test samples, the surface treatment of the aluminium adherend included abrasive sanding using P40 sandpaper followed by a cleaning process with ethanol solvent. A thin layer of Sika Primer 204N was also applied to favour the chemical bond at the adherend-adhesive interface. The adhesive thickness was controlled by using glass beads of a given diameter of 0.25 mm in the aluminium joints, and a clamping plates with fasteners in a designed grip as shown in [27, 28]. For the composite joints, the adherend were manually laid up and cured in an autoclave. A layer of peel ply was applied to the composite panel during the curing procedure to provide a contaminant free surface and the Onto^{TM} SB1050 treatment was applied to the adhesive overlap region before curing to promote chemical bonding interactions. All samples were cured in an oven at 120 ºC for 40 minutes.

The lap shear tests of the aluminium single lap joints were carried out using an Instron machine with a 30kN load cell, wedge-action grips, and a displacement rate of 1 mm/min at room temperature, as shown in Figure 3(a). For the aluminium joint, a mechanical extensometer was used to measure the relative displacement between the two dots (measuring reference points) at a distance of 12.5 mm to the adhesive overlap (as shown in Figure 1). For the composite joints, a laser extensometer was mounted at a defined distance and angle (5º) to measure the relative displacement (a distance of 12.5 mm to the adhesive overlap) between the two pads (with special tabs for the laser detector) attached to the bonded overlap area of the joints, as shown in Figure 3(b) [27, 28]. It can be seen that both two categories of joints failed in adhesion failure as shown in Figure 3(c) and 3(d), although a small area of delamination in the composite adherend was also observed (Figure 3(d)).

Figure 4 presents the comparison of the load-displacement curves of the identical aluminium and composite joints obtained from experiments and the corresponding FE models. A good agreement can be found by comparing the slopes of the curves to represent the stiffness of the joints, which demonstrates the accuracy of the modelling technique.

3. Machine Learning Models

3.1 Data points sampling

The principle of data-based approaches requires an appropriate data set from a specific problem domain for the purpose of accurate training and testing. It is expected that the selected data set can well represent the properties of the problem domain. In another words, it is better to have more averagely distributed data points in the problem domain. Therefore, sampling techniques are usually employed. Latin Hypercube Sampling (LHS) technique was used in this study, which has been widely employed by researchers [29]. Its superior efficiency over Mante Carlo Sampling (MCS) is well received. The detailed working principles of LHS can be found in previous studies [26, 29]. According to the principle of LHS, it is easy to find that the concept of random sampling in each stratified layer helps to prevent the generation of poor sampling areas. Hence, LHS method is expected to generate more representative samples than MCS method does.

In this study, seven design variables of single lap joint are defined as shown in Table 2, and four of which are continuous variables representing geometric features and the other three are discrete variables representing different material parameters. As shown in Table 2, parameters P1-P4 are the thickness of top and bottom adherends (T_1, T_2), bond overlap length (L_a) and the thickness of adhesive (T_a), respectively. The lower and upper bounds are defined for each parameter respectively, according to the published studies. The three discrete variables P5-P6 are the materials of the top adherend, bottom adherend and adhesive respectively. Integers (1 to

4) for the (top/bottom) adherends represent 4 different types of adherend materials (Polyphtalamide(PPA) [6], Aluminium 6082 T6, Woven CFRP [27, 28] and Steel Q235) as shown in Table 1(a). Integers (1 to 4) for the adhesive represent 4 different adhesive materials (AV138 [30], Araldite 2015 [30], Loctite EA 9497 [6] and FM94 [27, 28]) as shown in Table 1(b). Unlike the geometric parameters which are continuous values, the integer labels 1-4 represent corresponding material properties, which are discrete values.

Based on the definitions of these variables, LHS can be implemented to generate samples with different combinations of the variables. The algorithm of LHS is coded in the commercial software Matlab. In total, 300 sets of sample points are generated in the constrained domain. Then, the data sets are manually imported into Ansys Workbench, where 300 FE joint models with different geometry configurations and material definitions but same meshing strategy are automatically generated and solved. The corresponding FE simulation results are then used as the input data sets for the development of machine learning models.

3.2 Data pre-processing

To explore the problem systematically, the 300 sets of data should be processed by an appropriate pre-processing method before importing to machine learning models. The first step is to normalize the data of parameters P1-P4, since a normalized data set can regulate the whole data set at a same scale. The min-max normalization method was used in this analysis, since it is well known that the method usually has higher efficiency than *Z*-score normalization and decimal scaling normalization methods [31]. The min-max normalization is also called feature scaling which brings all parameters into the same range [0, 1], and it is formulated by:

$$X' = \frac{X - X_{min}}{X_{max} - X_{min}} \tag{1}$$

where X is the target parameter, and X' is the normalized data. X_{min} and X_{max} are the minimum and maximum values of the parameter X in the whole data set. Hence, the original data set can be transformed to a normalized data set, where each parameter is in the range [0, 1]. However, the three material parameters P5-P7 are not normalised. It is because that the three material parameters are discrete parameters that are defined by integers. And also they are of no necessity to be normalized in this study.

It is a common practice to split the 300 sets of normalized data into training and testing sets for the training and testing purposes in machine learning models. The data is split by a ratio 0.2 (20% of the whole set of data is testing data) which makes 240 sets of data fall into the training set and 60 sets of data fall into the testing set. In this study, *k*-fold cross-validation is employed to avoid the so-called 'overfitting' problem caused by a single random choice of the training and testing data in machine learning techniques [32]. The single parameter *k* refers to the number of groups that the data to be split into. In this study, three different groups of training and testing data are generated as shown in Figure 5. It follows the approach of 3-fold cross-validation but applies on a shuffled data set. In the 3 cross-validation groups, each contains 240 training sets and 60 testing sets. It also illustrates that each cross-validation group contains varied testing data, which are selected randomly. Then all the 3 groups of data are trained and tested in machine learning models, which will be developed in next sections.

3.3 Deep Neural Networks

ANN is a biological neural network inspired algorithm of which aim is to mimic a population of physically interconnected neurons or a group of disparate neurons [8]. Figure 6(a) shows a brief structure of a biological neuron. The biological neuron receives biological signals from the dendrites and modulate these signals in various amounts. The modulated information is output to the synapse as long as the strength of the signals reached a certain threshold. The principle of

an artificial neural network is depicted in Figure 6(b). All the input parameters obtained from the training data form the input layer of ANN. The information of these input parameters is modulated in the following hidden layer through an activation function *f(x)*. By this way, the weighted sum of the inputs is calculated to represent the total strength of the input signals. In addition, a step function is also used to evaluate if the strength has exceeded a certain threshold. When the strength exceeds the threshold, the information will be delivered to the output layers. By performing this method, ANN presents two key characteristics [33]: (1). It presents a strong ability in adaptive learning. (2). It learns knowledge from data by storing information in the weights of neurons. With these characteristics, ANN reveals its powerful capabilities in solving complicated regression and classification problems.

In this study, ANN is applied to reveal the hidden information and relationship between the seven joint parameters and the ultimate failure load of the joint. For describing this complicated relationship, an ANN structure with five hidden layers was developed as shown in Figure 7. As the structure becomes 'deeper' by having more than one hidden layer, the ANN structure is treated as a deep neural network (DNN). In the network, 260 sets of training data are input to the DNN model. These input parameters form up the input layer. Then, the information in the input layer is transferred to hidden layers by using weighted functions. The functions in the elliptical circle (Figure 7) depict how each hidden layer receives weighted information from its previous layer. It shows that the input information of the *i'th* neuron in the *j'th* hidden layer is the weighted sum of the information of all the neurons from the *(j-1)'th* layer. The w_i^j denotes the weight of the *i'th* neuron of the *j'th* layer, and b_j is the bias term which makes the network more flexible by adjusting the output along with the weighted sum of the inputs. Then the summed information z_i^j is regulated by the activation function δ, which is 'ReLU' in this case. The activation function can determine if the summed information of the current neuron should be activated or not. The same process performs at each layer and eventually all the information

is output to the terminal of the network. The terminal y_f is the output layer and it outputs the predicted failure load in this case.

The DNN model is coded by using Keras package in Python with the backend of Tensorflow. As shown in Table 3, the first hidden layer has 560 parameters as there are 7 input variables plus a bias term and then there are 70 elements in this layer plus additional 70 elements for the bias term. The parameters in the other layers can be calculated by the same way. The 'None' in the output shape indicates that there is no 2-dimensional input variable in this study. As a result, there are in total 4922 parameters and all of which are trainable parameters.

3.4 Genetic Programming

Genetic programming is an automated searching algorithm which is widely used to seek for reliable relationships between variables in a specific data set. Koza [34] firstly proposed the methodology of genetic programming in his article where he also mentioned its larger complexity over the traditional genetic algorithm. In genetic programming, populations are formed by computer programs and the programs can be represented by binary trees. Functions and terminals of the computer programs represent the branches and leaves of these binary trees. The working principal of genetic programming is exploiting, and its exploiting capability is inspired by Darwinian principle of natural selection and survival of the fittest [19]. The working principle of genetic programming is also illustrated in the previous article [26].

The working flowchart of the developed genetic programming model in this study is shown in Figure 8. The 300 sets of data are imported to train and test the genetic programming model. For each set of data, there are four continuous and three discrete variables and their corresponding simulation results of failure load of the bonded joint. Firstly, the program starts with an initialized population. At this stage, the initial population contains randomly generated computer programs, which attempt to describe the relationship between the input variables and

output results. Then, the fitness of this generation is evaluated and checked if it satisfies the terminate conditions. If it does not meet the terminate conditions, the first generation of programs becomes the parent generation. The parent generation will go through the processes of mutation and crossover of which aim is to evolve the programs. The evolved programs with higher fitness will be left and become the first children generation. It is deemed that the overall fitness of the children generation should be higher than its parent generation. The fitness of the first children generation will be evaluated to check if there is any program meets the terminate condition. If the terminate condition is not satisfied, the first children generation will turn to be the second parent generation and go through the processes of mutation and crossover again to generate the second children generation. As a result, the whole evolving process will run repeatedly if the terminate condition is not satisfied. When the fitness of a generation meets the terminate condition or the evolution has completed a defined number of generations, the whole process will stop. At the end, the programs in the final generation are expected having the best fitness, which should have a good ability to predict the ultimate failure force F_s by giving the 7 variables.

In this study, the genetic programming method is coded using the package 'GPlearn' in Python. The specific parameters of the genetic programming model for this case are shown in Table 4. The population is initialized with the size of 6000 and the maximum number of evolution generations is 200. The stopping criteria is 0.01. It can early stop the program when the terminate condition is satisfied. And the chances of crossover and mutation are 0.7 and 0.25 respectively. The parsimony coefficient is 2e-5 to control the overall length of the generated programs in each generation.

4. Results and Discussion

4.1 Results of machine learning models

To avoid "over-fitting", three groups of data which were pre-processed by 3-fold cross validation method, are used in developing both two machine learning models. Each group of data is randomly divided by the ratio of 0.2. The validation of the training results of the DNN model on the 3 different groups of data are shown in Figure 9(a-c) respectively. The points in all the three charts are close to the validation lines. It illustrates that the training accuracy of the developed DNN model remains at a high level, although the data is varying in the different groups. The testing data and the DNN predicted results of the three validation groups are displayed in Figure 9(d-f) respectively. The testing results are all very close to the validation line though slight difference can be observed between different groups. A widely used method for evaluating the prediction accuracy is to calculate the *R* squared (R^2) value. The definition of R^2 is expressed by:

$$R^2 = 1 - \frac{\sum_i (y_i - f_i)^2}{\sum_i (y_i - \bar{y})^2} \tag{2}$$

where y_i is the value of the *i'th* testing data point, and $\bar{y}$ is the mean value of the testing data. f_i denotes the value of the *i'th* predicted data point. Hence, R^2 represents the proportion of the variance for a dependent variable that is explained by the fitting model, or simply saying the goodness-of-fit. In Figure 9(d-f), the R^2 are 0.939, 0.892 and 0.951 for the predictions of the three groups of testing sets. Despite of the slight difference, the results show that the ultimate failure loads of the joints are accurately predicted by the developed DNN model. The accurate prediction rates of the 3 different cross-validation groups indicate that the DNN model does not have the problem of over-fitting. It ensures the accuracy of the developed model regardless of the different selections of data sets.

Similarly, the training results based on the developed GP model are shown in Figure 10(a-c) for the three cross-validation groups respectively. Nearly all the points are concentrated along the validation line, which shows good training accuracies. Compared with the training results of the DNN model (Figure 9(a-c)), the GP model shows similar training rate on all the three data groups. Figure 10(d- f) show the testing results of the three different groups based on the GP model, and the corresponding R^2 values are 0.934, 0.909 and 0.939 respectively. Compared to the testing R^2 values for the three groups (0.939, 0.892 and 0.951) based on the DNN model, the accuracies of the first and last data groups based on GP model are slightly lower but the accuracy of the second data group is a bit higher than that of DNN model. On the other hand, both the DNN model and the GP model show high prediction accuracies on all the three cross-validation groups though the accuracy of Group 02 is slightly lower than the accuracies of the other two groups. In general, it demonstrates that both the DNN model and the GP model present good prediction accuracies on the given data sets without any over-fitting problems.

As both the machine learning models perform successfully on all the three groups of data sets, the data set of Group 01 is selected to train both the models. Although having similar prediction accuracies, the GP and the DNN methods actually give out different types of prediction models. Based on the data Group 01, the GP method generates a function:

$$f(x_1, x_2, x_3, x_4, x_5, x_6, x_7) = 2.5e^{-3} A_2 \cdot \sqrt{\left| x_3 \cdot x_6 \cdot \left(\sqrt{|A_5|} \cdot A_3 + x_5 - 0.272 \right) \right|} \quad (3)$$

where:

$$A_1 = \sqrt{| - x_1 + 7.84e^{-4}(x_4 + x_5 - x_7) - 2.13e^{-4}|}$$

$$A_2 = \sqrt{|\sqrt{x_3} - x_3 + x_4 \cdot (\sqrt{x_3} + x_4 + x_5 - 2x_7 + 0.028)|}$$

$$A_3 = 0.028x_1 \cdot (\frac{x_2}{x_4} + x_7)$$

$$A_4 = x_6 - 0.028\sqrt{|x_3(-x_1 + (x_5 + 0.028x_7) \cdot A_1)|}$$

$$A_5 = 0.028 \cdot \left(x_5 - 3x_7 + \frac{A_4}{x_7 - 1.03}\right) \cdot (x_5 - 0.272x_6 + 0.028x_7)$$

The joint failure load $f(x_1, x_2, x_3, x_4, x_5, x_6, x_7)$ is formulated by the variables $x_1 - x_7$ which represent the four continuous variables P1-P4 and three discrete variables P5-P7 respectively as shown in Table 2. The generated function is one of the viable solutions searched by the GP algorithm to fit the real relationship between the ultimate failure load and the geometry/material parameters of the joint. On the contrary, the DNN model cannot give out a visible function to depict the relationship between the input parameters and the output results, though it can perform as well as the GP model does on predicting the joint failure load. It is because the characteristics of a DNN model is to find the relationships between inputs and outputs by constructing complicated layers. These layers make the DNN model possible to fit the data that has nonlinear internal relationships. However, it also makes the model too complicated to give out a visible expression. Therefore, it can be concluded that the DNN model can be treated as a black box model as it gives no knowledge of the internal structure of the model, whilst the GP model is more like a grey box which contains a part knowledge of the whole problem. However, both the developed GP and DNN models could be used as tools for design and analysis of adhesive joints in many practical scenarios, such as, geometry optimization and material selection.

4.2 Selection of adhesive and design of adhesive layer for a hybrid joint

One of the most common scenarios in designing an adhesive joint is to determine the right adhesive and the configuration of the adhesive layer for two given adherends. In practice, when

the materials and geometries of the top and bottom adherends are determined, it is necessary to choose a right adhesive and determine the corresponding thickness and length of the adhesive layer to ensure an optimal joint strength. In the case study, it assumes that the materials of the top adherend is PPA and the bottom adherend is Al, of which properties are shown in Table 1(a). The thicknesses of the top and bottom adherends are both 3 mm, which has been widely used in structural components. Hence, in the ML models, the input variables P1 and P2 are assigned by the value of 3 and the discrete variables P5 and P6 are equal to 1 and 2 respectively. As a result, for a given adhesive P7, only two variables P3 and P4, which represent the length and the thickness of the adhesive layer (Table 2), are left in the models. Then, the corresponding failure loads of the joint can be discussed by both DNN and GP models with the values of P3 and P4 varying in their own bounds.

The results of joint failure load predicted by the developed DNN model with respect to the length P3 and the thickness P4 of the four different adhesives are plotted in Figure 11. For all the four different adhesive materials, the relationships are plotted as curved surfaces, but they all contain the similar trend that the predicted failure loads increase when the thickness of adhesive decreases and the length of adhesive increases. It is also found that the peak force predicted by the DNN model for the joint with AV138 adhesive (P7=1) is around 1900 N, and the values are around 1450 N, 1600 N and 1850 N for the joints with Araldite 2015 (P7 = 2), Loctite EA 9497 (P7 = 3) and FM94 (P7 = 4), respectively. According to the prediction results based on the DNN model, the suggest adhesive for the PPA/AL joint is AV138 adhesive (P7=1), and thickness of the adhesive is suggested to be as thin as possible (approach to 0.1 mm), and the length of adhesive approaches to 70 mm. This is because this design gives an approximately 1900 N peak failure load which is higher than the possible designs with other three adhesives.

The three-dimensional plots of the failure loads predicted by the GP model with respect to the length P3 and the thickness P4 of the adhesive for four different adhesive materials are shown in

Figure 12. The plots demonstrate a similar trend as obtained by the DNN model, where the predicted failure loads increase, when the thickness of adhesive decreases and the length of adhesive increases. However, the shape of the curved surfaces obtained by the GP model is slightly different from the ones based on the DNN model. For the results of GP, when the thickness of the adhesive is larger than 0.5 mm and the adhesive length is smaller than 50 mm, the surface tends to be flatter which illustrates that the failure load tends to have lower nonlinear relationships with the two variables. When the thickness of the adhesive is smaller than 0.5 mm and the length is larger than 50 mm, a significant increment can be observed on the plot surfaces. It is because that the GP model tends to use combined linarites and nonlinearities to depict the relationships in the whole area. On the contrary, the DNN model tries to represent the relationships between the variables and the output by assuming global nonlinearities. Therefore, the DNN model manages to predict the results and have smooth transitions on the whole results surfaces, while on the results surfaces based on the GP model, there are more clear boundaries to differentiate linear and nonlinear areas. The predicted failure loads for AV138 adhesive (P7=1), Araldite 2015 (P7 = 2) and Loctite EA 9497 (P7 = 3) are around 1900 N, 1400 N and 1500 N, respectively, which are similar to the values obtained by the DNN model. For FM94 (P7 = 4), the peak failure load predicted by the GP model is 1600 N which is approximate 200 N lower than the value predicted by the DNN model. Despite the slight difference, the suggested design based on the GP is same to the one suggested by the DNN model. For the PPA/AL joint, AV138 adhesive (P7=1) with the very thin thickness and the overlap length approaching to 70 mm is the suggested optimal design, which gives a peak failure load close to 1900 N.

5. Conclusion

Two machine learning models (GP and DNN) are developed in this study to predict the ultimate failure load of single lap joints by considering four continuous geometry variables and three

discrete material variables. The data sets for training and testing the machine learning models are selected by employing the DoE method Latin Hypercube Sampling (LHS). To generate the data set for the machine learning models, a parametric FE model is developed in Ansys Workbench and validated by two different experimental tests. In total, 300 sets of data are generated by the developed parametric FE model, 240 sets of which are used to train the models and the rest 60 sets are used for testing. In order to avoid the over-fitting problem, the 3-fold cross-validation method is employed. The developed GP model acts as a grey-box model which can give out a visible expression to show the relationships between the variables and the output. The DNN model is, on the contrary, a total black-box model of which internal structure of the solution is very complicated and invisible. But the results show that both the DNN and GP methods have robust abilities for accurately predicting the failure load of a single-lap joint by considering both continuous geometry variables and discrete material variables. Therefore, both the developed DNN and GP models can be used in practice as a tool to analyse and design adhesive single lap joints. Moreover, the results may also indicate that other similar machine learning methods, such as adaptive neuro-fuzzy inference system (a kind of artificial neural network based on Takagi-Sugeno fuzzy inference system), which has been applied in predicting performance of composite laminates [35, 36], could be also potentially used in this field.

In the case study of designing adhesive layer for a hybrid PPA-Al joint, both the models conclude a similar trend on the effects of the adhesive selection and geometry configurations of the adhesive layer on comparing the final failure load of the joint. And an agreed optimal design for the hybrid joint is suggested by both the ML models, which uses AV138 adhesive, and the thickness and length of the adhesive layer should be closed to 0.1 mm and 70 mm respectively. Actually, the developed models can be also used in other scenarios in practical design. By fixing the values of the confirmed design variables, the relationships between the uncertain variables and the failure load can be analysed, and the optimal design could be determined.

References

[1] Herrmann C, Dewulf W, Hauschild M, Kaluza A, Kara S, Skerlos S. Life cycle engineering of lightweight structures. CIRP Annals. 2018;67(2):651-72.
[2] Budhe S, Banea M, De Barros S, Da Silva L. An updated review of adhesively bonded joints in composite materials. International Journal of Adhesion and Adhesives. 2017;72:30-42.
[3] Da Silva LF, Carbas R, Critchlow GW, Figueiredo M, Brown K. Effect of material, geometry, surface treatment and environment on the shear strength of single lap joints. International Journal of Adhesion and Adhesives. 2009;29(6):621-32.
[4] Mokhtari M, Madani K, Belhouari M, Touzain S, Feaugas X, Ratwani M. Effects of composite adherend properties on stresses in double lap bonded joints. Materials & Design. 2013;44:633-9.
[5] Liao L, Huang C, Sawa T. Effect of adhesive thickness, adhesive type and scarf angle on the mechanical properties of scarf adhesive joints. International Journal of Solids and Structures. 2013;50(25-26):4333-40.
[6] Kanani AY, Liu Y, Hughes DJ, Ye J, Hou X. Fracture mechanisms of hybrid adhesive bonded joints: Effects of the stiffness of constituents. International Journal of Adhesion and Adhesives. 2020;102:102649.
[7] Han X, Chao Y, Zhang W, Chao Y, Wu C. Study on the effect of post curing on the mode II fracture energy of structural adhesive using a parameter identification approach. International Journal of Adhesion and Adhesives. 2019;95:102398.
[8] McCulloch WS, Pitts W. A logical calculus of the ideas immanent in nervous activity. The bulletin of mathematical biophysics. 1943;5(4):115-33.
[9] Mashrei MA, Seracino R, Rahman M. Application of artificial neural networks to predict the bond strength of FRP-to-concrete joints. Construction and Building Materials. 2013;40:812-21.
[10] Tosun E, Calık A. Failure load prediction of single lap adhesive joints using artificial neural networks. Alexandria Engineering Journal. 2016;55(2):1341-6.
[11] Balcıoğlu HE, Seçkin AÇ, Aktaş M. Failure load prediction of adhesively bonded pultruded composites using artificial neural network. Journal of Composite Materials. 2016;50(23):3267-81.
[12] Rangaswamy H, Sogalad I, Basavarajappa S, Acharya S, Manjunath Patel G. Experimental analysis and prediction of strength of adhesive-bonded single-lap composite joints: Taguchi and artificial neural network approaches. SN Applied Sciences. 2020;2:1-15.
[13] Forsyth R. Beagle-a Darwinian approach to pattern recognition. Kybernetes. 1981;10(3):159-66.
[14] Cevik A, Arslan MH, Köroğlu MA. Genetic-programming-based modeling of RC beam torsional strength. KSCE Journal of Civil Engineering. 2010;14(3):371-84.
[15] Cevik A. Genetic programming based formulation of rotation capacity of wide flange beams. Journal of Constructional Steel Research. 2007;63(7):884-93.
[16] Gandomi AH, Tabatabaei SM, Moradian MH, Radfar A, Alavi AH. A new prediction model for the load capacity of castellated steel beams. Journal of Constructional Steel Research. 2011;67(7):1096-105.

[17] Pala M. Genetic programming-based formulation for distortional buckling stress of cold-formed steel members. Journal of Constructional Steel Research. 2008;64(12):1495-504.
[18] Beiki M, Bashari A, Majdi A. Genetic programming approach for estimating the deformation modulus of rock mass using sensitivity analysis by neural network. International journal of rock mechanics and mining sciences. 2010;47(7):1091-103.
[19] Assimi H, Jamali A, Nariman-Zadeh N. Sizing and topology optimization of truss structures using genetic programming. Swarm and evolutionary computation. 2017;37:90-103.
[20] Gandomi AH, Alavi AH. A new multi-gene genetic programming approach to nonlinear system modeling. Part I: materials and structural engineering problems. Neural Computing and Applications. 2012;21(1):171-87.
[21] Huang Z, Deng W, Du S, Gu Z, Long W, Ye J. Effect of rubber particles and fibers on the dynamic compressive behavior of novel ultra-lightweight cement composites: Numerical simulations and metamodeling. Composite Structures. 2020:113210.
[22] Liu D, Zhou X, Toropov V. Metamodels for composite lattice fuselage design. International Journal of Materials, Mechanics and Manufacturing. 2016;4(3):175-8.
[23] Luo L, Liu D, Zhu M, Ye J. Metamodel-assisted design optimization of piezoelectric flex transducer for maximal bio-kinetic energy conversion. Journal of Intelligent Material Systems and Structures. 2017;28(18):2528-38.
[24] Luo L, Liu D, Zhu M, Liu Y, Ye J. Maximum energy conversion from human motion using piezoelectric flex transducer: A multi-level surrogate modeling strategy. Journal of Intelligent Material Systems and Structures. 2018;29(15):3097-107.
[25] Al-Mosawe A, Kalfat R, Al-Mahaidi R. Strength of Cfrp-steel double strap joints under impact loads using genetic programming. Composite Structures. 2017;160:1205-11.
[26] Liu Y, Gu Z, Hughes DJ, Ye J, Hou X. Understanding mixed mode ratio of adhesively bonded joints using genetic programming (GP). Composite Structures. 2020:113389.
[27] Liu Y, Lemanski S, Zhang X, Ayre D, Nezhad HY. A finite element study of fatigue crack propagation in single lap bonded joint with process-induced disbond. International Journal of Adhesion and Adhesives. 2018;87:164-72.
[28] Liu Y, Zhang X, Lemanski S, Nezhad HY, Ayre D. Experimental and numerical study of process-induced defects and their effect on fatigue debonding in composite joints. International Journal of Fatigue. 2019;125:47-57.
[29] Olsson AM, Sandberg GE. Latin hypercube sampling for stochastic finite element analysis. Journal of Engineering Mechanics. 2002;128(1):121-5.
[30] Campilho RD, Banea MD, Neto J, da Silva LF. Modelling adhesive joints with cohesive zone models: effect of the cohesive law shape of the adhesive layer. International journal of adhesion and adhesives. 2013;44:48-56.
[31] Mohd Nawi N, Atomia WH, Rehman MZ. The effect of data pre-processing on optimized training of artificial neural networks. 2013.
[32] Donate JP, Cortez P, SáNchez GG, De Miguel AS. Time series forecasting using a weighted cross-validation evolutionary artificial neural network ensemble. Neurocomputing. 2013;109:27-32.

[33] Jiang K, Han Q, Bai Y, Du X. Data-driven ultimate conditions prediction and stress-strain model for FRP-confined concrete. Composite Structures. 2020:112094.
[34] Koza JR, Koza JR. Genetic programming: on the programming of computers by means of natural selection: MIT press; 1992.
[35] Vassilopoulos AP, Bedi R. Adaptive neuro-fuzzy inference system in modelling fatigue life of multidirectional composite laminates. Computational Materials Science. 2008;43(4):1086-93.
[36] Mesbahi AH, Semnani D, Khorasani SN. Performance prediction of a specific wear rate in epoxy nanocomposites with various composition content of polytetrafluoroethylen (PTFE), graphite, short carbon fibers (CF) and nano-TiO2 using adaptive neuro-fuzzy inference system (ANFIS). Composites Part B: Engineering. 2012;43(2):549-58.

Figures

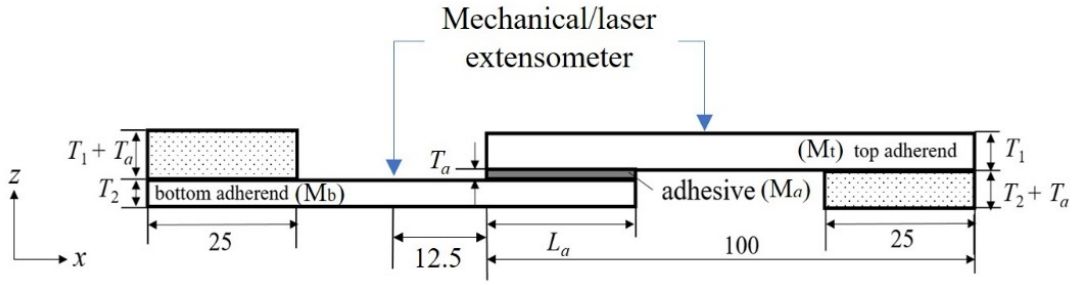

Figure 1: Geometry and dimensions of parametric single lap joint FE model with width of 25 (unit: mm)

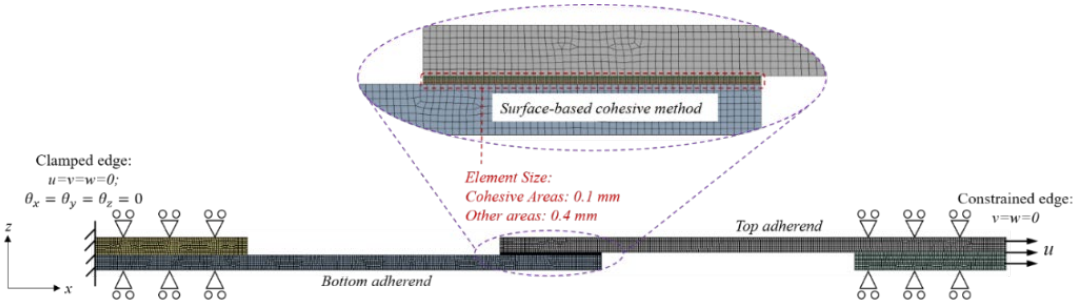

Figure 2: Load and boundary conditions of single lap joint FE model

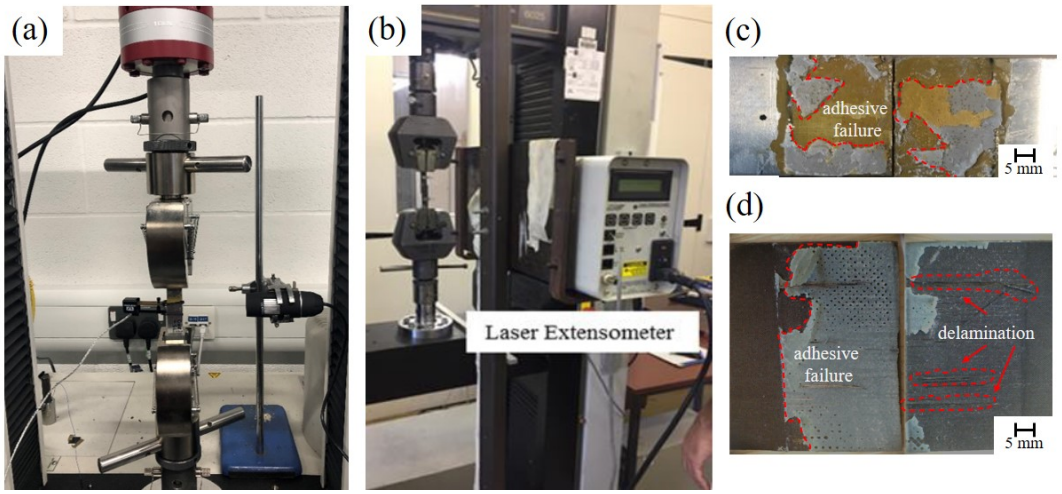

Figure 3: The setup of the test machine with (a) mechanical extensometer and (b) laser extensometer, and the failure of identical (c) aluminium joints and (d) composite joints.

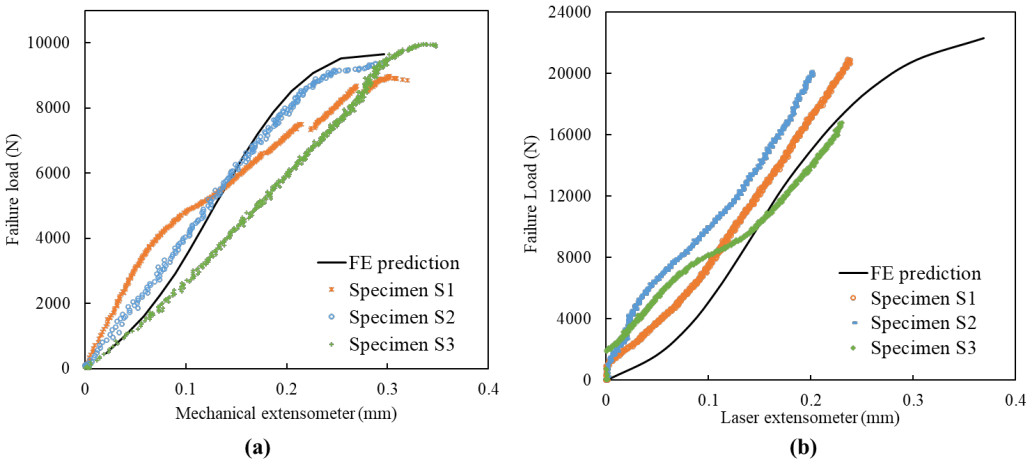

Figure 4: Load-displacement curves of identical (a) aluminium and (b) composite joints

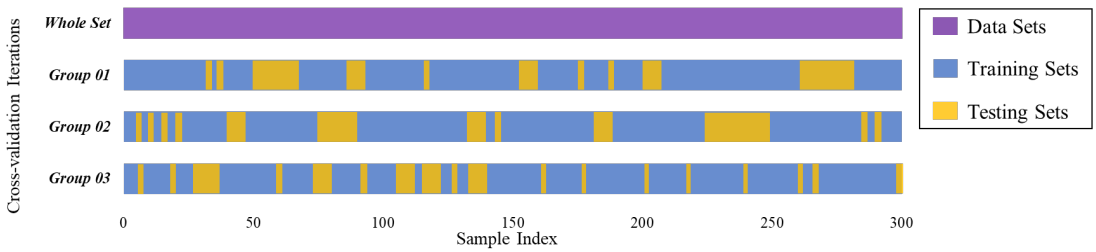

Figure 5: Training and testing data sets divisions split by random 3-fold cross-validation method.

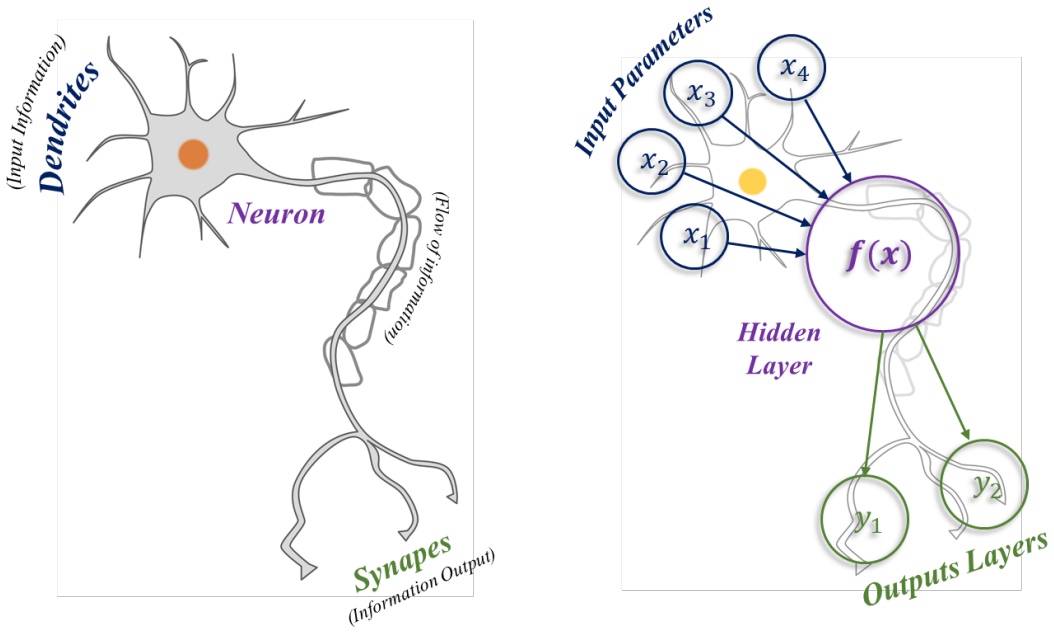

Figure 6: The schematic of how artificial neuron networks mimic the function of biological neuron networks.

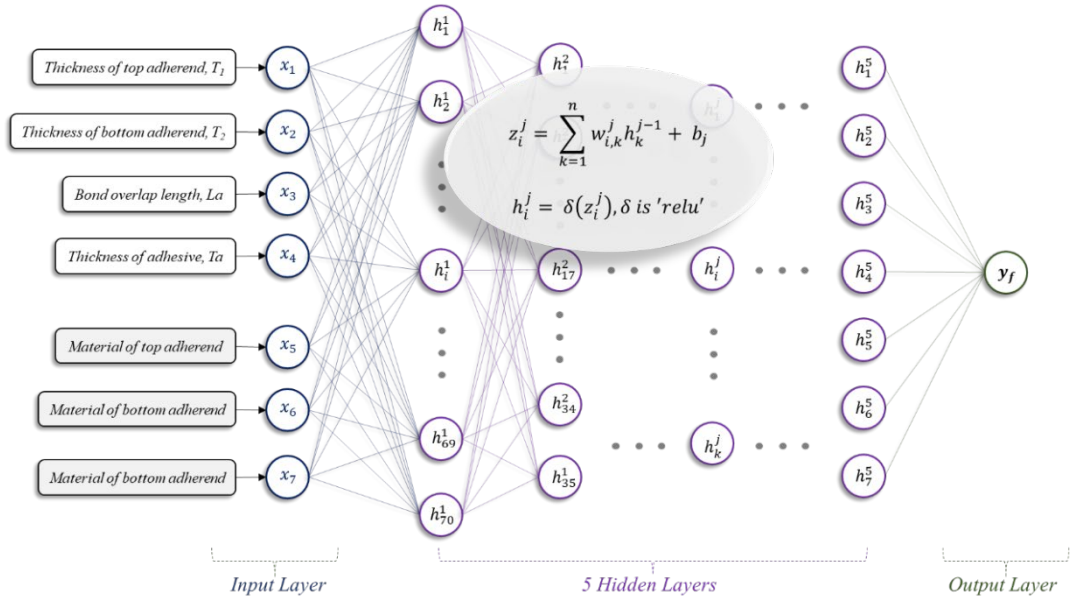

Figure 7: General schematic of a deep neuron network for predicting ultimate failure load of a single lap joint

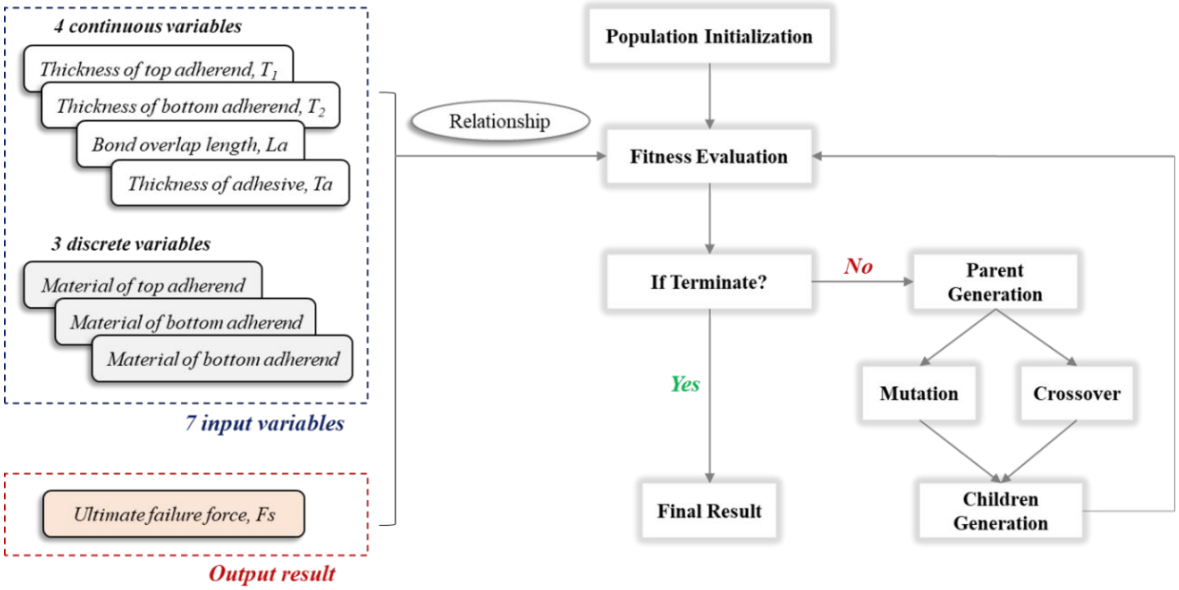

Figure 8: Flowchart of how genetic programming technique applies on the continuous and discrete variables of single lap joints.

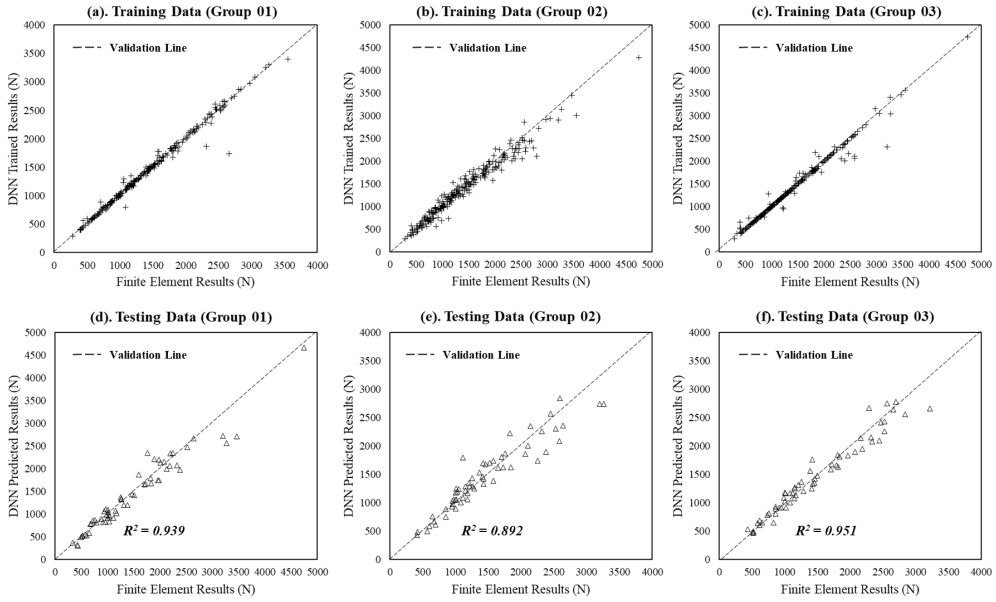

Figure 9: Comparisons of the training results of the ultimate failure load for cross-validation (a). Group 01, (b). Group 02 and (c). Group 03, and the testing results of the failure load for cross-validation (d). Group 01, (e). Group 02 and (f). Group 03 based on the DNN Model.

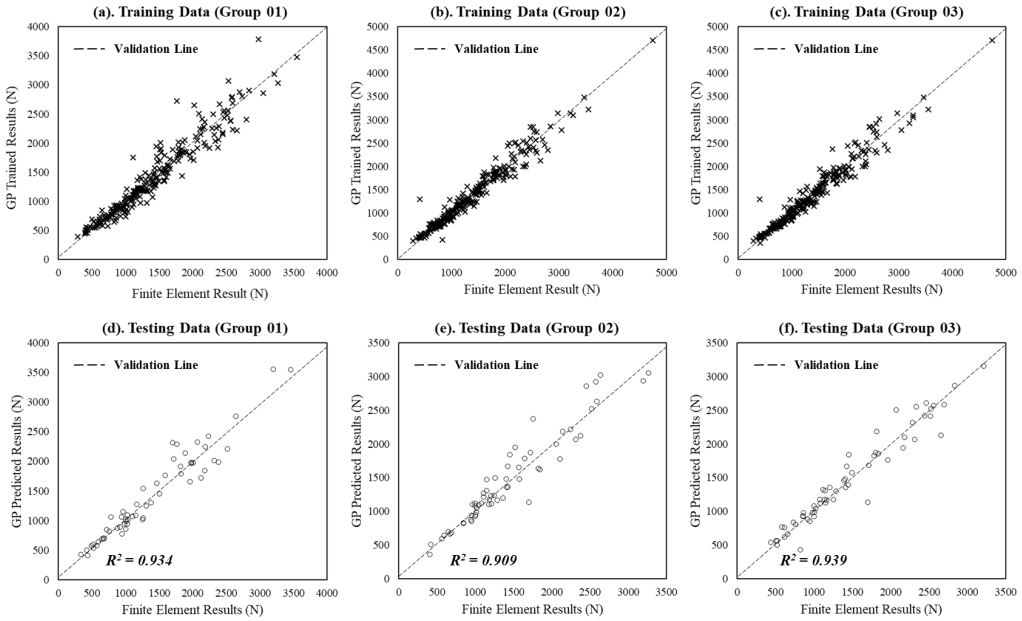

Figure 10: Comparisons of the training results of the ultimate failure load for cross-validation (a). Group 01, (b). Group 02 and (c). Group 03, and the testing results of the failure load for cross-validation (d). Group 01, (e). Group 02 and (f). Group 03 based on the GP Model.

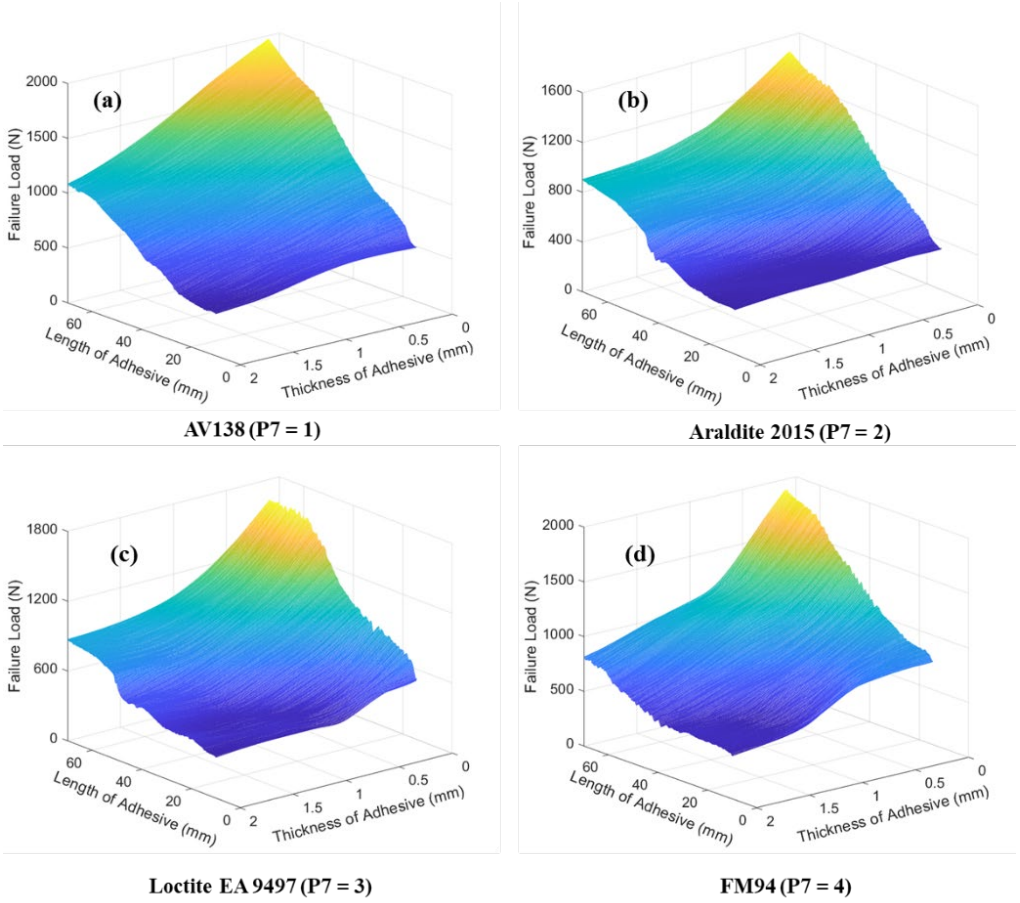

Figure 11: Three-dimensional plotting of the effects of the length and the thickness of adhesive on 4 different adhesive materials: (a) AV138 (P7=1), (b) Araldite 2015 (P7=2), (c) Loctite EA 9497 (P7=3) and (d). FM94 (P7=4) based on the DNN model.

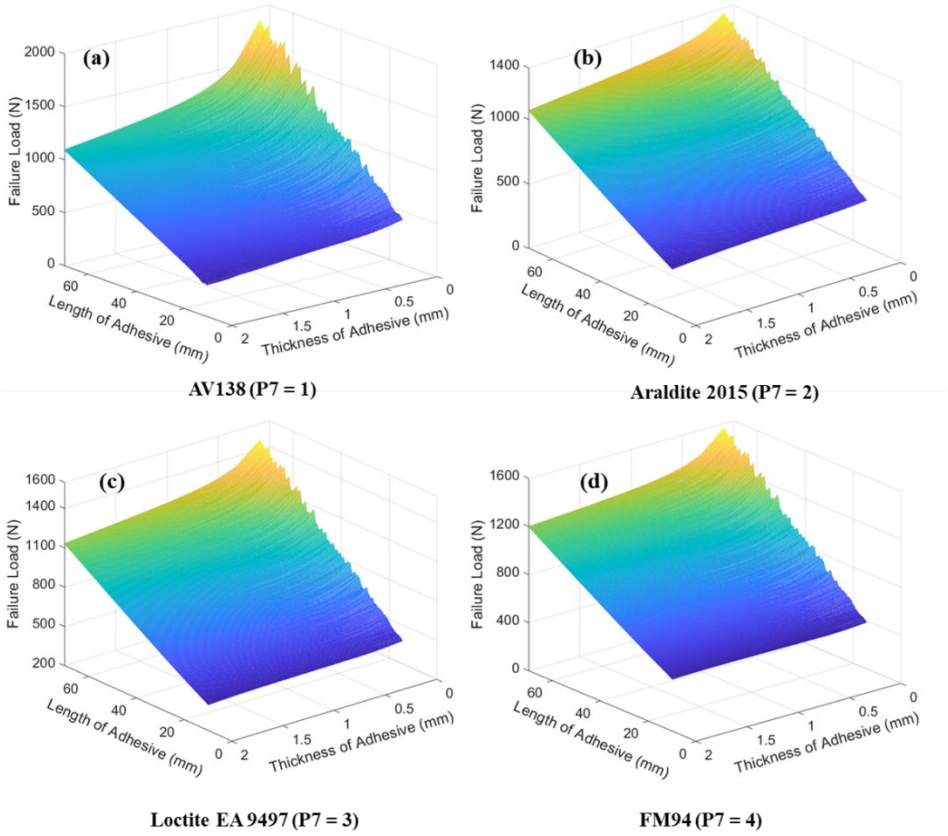

Figure 12: Three-dimensional plotting of the effects of the length and the thickness of adhesive on 4 different adhesive materials: (a) AV138 (P7=1), (b) Araldite 2015 (P7=2), (c) Loctite EA 9497 (P7=3) and (d). FM94 (P7=4) based on the GP model.

Tables

Table 1: Material properties of (a). top and bottom adherends, and (b). adhesives.

(a). Materials of top and bottom adherends.

	Polyphtalamide (PPA) (50% glass fibre) [6]	**Aluminium 6082 T6**	**Woven CFRP** [27, 28]	**Steel Q235**
Label Number	*1*	*2*	*3*	*4*
Young's Modulus, E (GPa)	*17.62*	*70.00*	*76.39*	*210.00*
Poisson's Ratio, v	*0.32*	*0.30*	*0.40*	*0.30*

(b). Adhesives.

	AV138 [30]	**Araldite 2015** [30]	**Loctite EA 9497** [6]	**FM94** [27, 28]
Label Number	*1*	*2*	*3*	*4*
Young's modulus, E (MPa)	*4890*	*1850*	*7710*	*3000*
Poisson's ratio, v	*0.35*	*0.33*	*0.29*	*0.35*
Tensile failure strength, σ_f (MPa)	*39.45*	*21.63*	*25.35*	*30.00*
Shear failure strength, τ_f (MPa)	*30.20*	*17.90*	*16.00*	*20.00*
Toughness in tension, G_{IC} (N/mm)	*0.20*	*0.43*	*0.26*	*1.50*
Toughness in shear, G_{IIC} (N/mm)	*0.38*	*4.70*	*0.90*	*2.70*

Table 2: Continuous geometry parameters and discrete materiel parameters of a single lap joint.

	Parameters (LHS)	Lower Bound	Upper Bound	Symbol
Continuous Values (mm)	*Thickness of top adherend, T_1*	*1*	*10*	*P1*
	Thickness of bottom adherend, T_2	*1*	*10*	*P2*
	Bond overlap length, L_a	*10*	*70*	*P3*
	Thickness of adhesive, T_a	*0.1*	*2*	*P4*
Discrete Values	*Material of top adherend M_t*	*1*	*4*	*P5*
	Material of bottom adherend M_b	*1*	*4*	*P6*
	Material of adhesive M_a	*1*	*4*	*P7*

Table 3: Structure of layers and elements in the generated DNN model.

Layer (Type)	Output Shape	Parameters (DNN Layers)
Input Layer	(None, 7)	7
Hidden Layer 01 (Dense)	(None, 70)	560
Hidden Layer 02 (Dense)	(None, 35)	2485
Hidden Layer 03 (Dense)	(None, 35)	1260
Hidden Layer 04 (Dense)	(None, 14)	504
Hidden Layer 05(Dense)	(None, 7)	105
Output Layer (Dense)	(None, 1)	1

Total Parameters: 4, 922, Trainable Parameters: 4, 922

Table 4: Settings of genetic programming model by using 'GPlearn' in Python

Parameters (GPlearn)	Function set	Population size	Generations	Parsimony coefficient
Values	*'+', '-', '*', '/', '√'*	*6000*	*200*	*2e-5*

Parameters (GPlearn)	Crossover	Subtree mutation	Hoist mutation	Point mutation
Values	*0.7*	*0.1*	*0.05*	*0.1*